nanomaterials

MDPI

Article

Ionic Transportation and Dielectric Properties of YF_3:Eu^{3+} Nanocrystals

Xiaoyan Cui [1], Tingjing Hu [1,*], Jingshu Wang [1], Junkai Zhang [1], Xin Zhong [1], Yanli Chen [1], Xuefei Li [1], Jinghai Yang [1] and Chunxiao Gao [2]

[1] Key Laboratory of Functional Materials Physics and Chemistry of the Ministry of Education, National Demonstration Center for Experimental Physics Education, Jilin Normal University, Siping 136000, China; xycuimail@163.com (X.C.); jingshuwang126@126.com (J.W.); junkaizhang126@126.com (J.Z.); zhongxin@calypso.cn (X.Z.); chenqian358@126.com (Y.C.); xuefeili163@163.com (X.L.); jhyang1@jlnu.edu.cn (J.Y.)

[2] State Key Laboratory of Superhard Materials, Jilin University, Changchun 130012, China; chunxiaogao126@126.com

* Correspondence: tjhumars@126.com

Received: 16 November 2018; Accepted: 29 November 2018; Published: 1 December 2018

Abstract: The ionic transportation and dielectric properties of YF_3:Eu^{3+} nanocrystals are investigated by AC impedance spectroscopy. The ion diffusion coefficient and conductivity increase along with the doping concentration and reach their highest values at 4% of Eu^{3+}. The difference of ionic radius between Eu^{3+} and Y^{3+} leads to the structural disorder and lattice strain, which deduces the increase of the ion diffusion coefficient and conductivity before 4% Eu^{3+} doping; then the interaction of the neighboring doping ions is dominated, which results in the difficulty of ion migration and decreases of the ion diffusion coefficient and conductivity. The strong dispersion of the permittivity in the low frequency region indicates that the charge carrier transport mechanism is the ion hopping in the system. The low-frequency hopping dispersion is affected by an interfacial polarization, which exhibits a Maxwell-Wagner relaxation process, and its loss peak shifts to higher frequency with the ionic conductivity increasing.

Keywords: nanocrystals; ionic transportation; dielectric behavior; permittivity

1. Introduction

Rare-earth fluoride nanomaterials have attracted a great deal of interest due to their unique physical and chemical properties and potential applications in luminescence, optoelectronic, down/up conversion devices, etc. [1–6]. Among the rare earth fluorides, YF_3 is an important material and has widespread potential applications in optical telecommunication, phosphors, down/up conversion luminescent devices, solid-state batteries, sensors [6–14], etc. Due to the closed ionic radius and the same valence, the Y^{3+} can be easily replaced by other rare earth ions [15,16]. Moreover, YF_3 has low refractive index and wide bandgap [17,18]. Therefore, YF_3 is an attractive host material for lanthanide-doped phosphors. At the same time, due to its high ionic conduction, YF_3 is a prospective material used as a solid electrolyte of solid-state electrochemical devices.

As the phosphor host and solid electrolyte material, the ionic conductivity and dielectric properties of YF_3 nanocrystals are important subjects. Many investigations have been focused on the structure, synthesis and optical properties of YF_3 nanocrystals [8–11,19–21]. However, few reports have been conducted on the electrical and dielectric properties of YF_3. Only Sathyamoorthy et al. have investigated the AC conduction of YF_3 thin film, whose structure is amorphous [22]. A thorough study on the carrier transport and dielectric properties of YF_3 nanocrystals is necessary. In this letter, the ionic

transportation and dielectric properties of YF_3:Eu^{3+} nanocrystals are investigated by AC impedance spectroscopy. The ionic diffusion, ionic conductivity and complex permittivity are discussed with various Eu^{3+} doping concentrations.

2. Materials and Methods

The synthetic process of YF_3:Eu^{3+} nanocrystal is similar to that of alkaline earth fluorides [23–26]. The mixed solution of oleic acid, ethanol and ammonia was stirred for 10 min; then 3.0641 g $Y(NO_3)_3 \cdot 6H_2O$ and 0.7402 g NH_4F were added and stirred thoroughly. The above solution was put into an autoclave and then reacted for 24 h at 190 °C. The final production was obtained through centrifugation, washing and drying. The Eu^{3+}-doping samples was obtained by replacing $Y(NO_3)_3$ with a certain amount of $Eu(NO_3)_3$ and the Eu^{3+} doping concentrations are 2, 4, 6, 8, 10 mol% respectively. The morphology and particle size of sample were obtained by transmission electron microscope (TEM). The structure and component of sample were obtained by X-ray diffraction (XRD) and energy dispersive spectrometer (EDS). The detailed measurement process of AC impedance spectroscopy was described in our previous works [27,28]. The spectra were measured by parallel plate electrode. The copper sheet was used as electrode, which is an ions' blocking material. The sample chamber is a cylinder (ø6 mm × 1 mm). The amplitude of AC voltage needs to be selected according to the sample. Though our testing, the appropriate input voltage for this sample is 1 V. The frequency is 0.01–10^7 HZ.

3. Results and Discussion

The structure, component and morphology of YF_3 with different Eu^{3+}-doping concentrations were investigated by XRD, EDS and TEM as shown in Figures 1–3. It can be seen that all the XRD spectra can be indexed as orthorhombic YF_3 structure (JCPDS Card No. 74-0911), and the existence of Eu peak in the EDS spectra proves that the Eu^{3+} ion successfully replaces Y^{3+} in the Eu^{3+}-doping samples. The TEM results show that all the samples are well crystallized and all of their particle sizes are about 28 ± 4 nm.

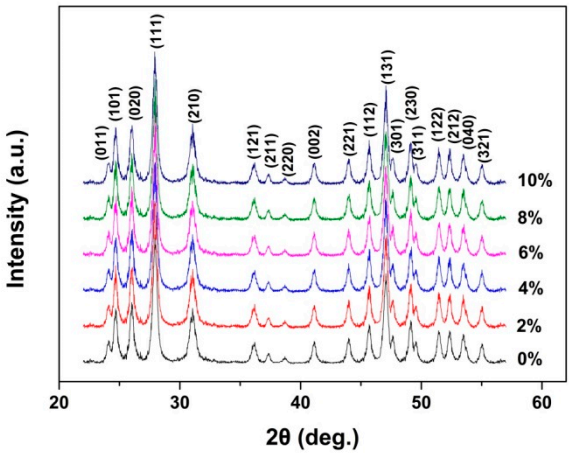

Figure 1. The XRD spectrum of YF_3:Eu^{3+} nanocrystals.

The impedance plots of YF_3 with different Eu^{3+}-doping concentrations are shown in Figure 4. It shows that all the spectra display a semicircle and a straight line. To obtain the transport parameters, the impedance spectra are usually analyzed by the equivalent circuits. The straight line indicates the existence of the Warburg diffusion process [29]; therefore, a Warburg element was added into the equivalent circuit. The equivalent circuit we used was shown in the insert of Figure 4 and the fitting parameters for the impedance plots were listed in Table 1. The good agreements of the impedance spectra and the simulate plots indicate that the equivalent circuit is appropriate.

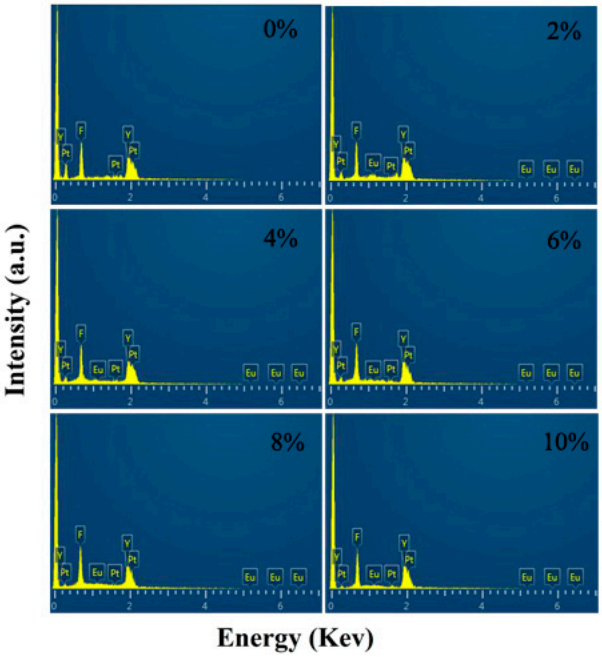

Figure 2. The EDS spectrum of YF_3:Eu^{3+} nanocrystals.

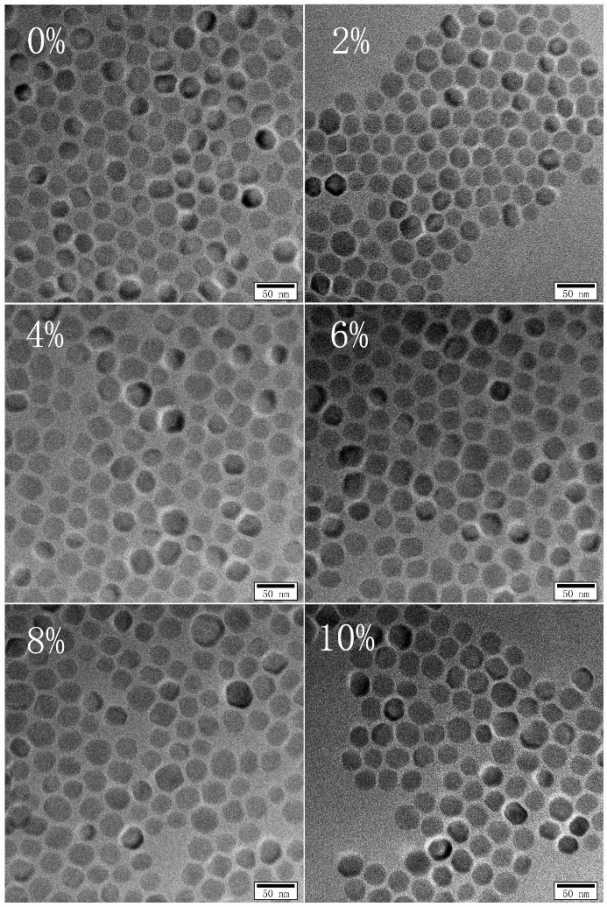

Figure 3. *Cont.*

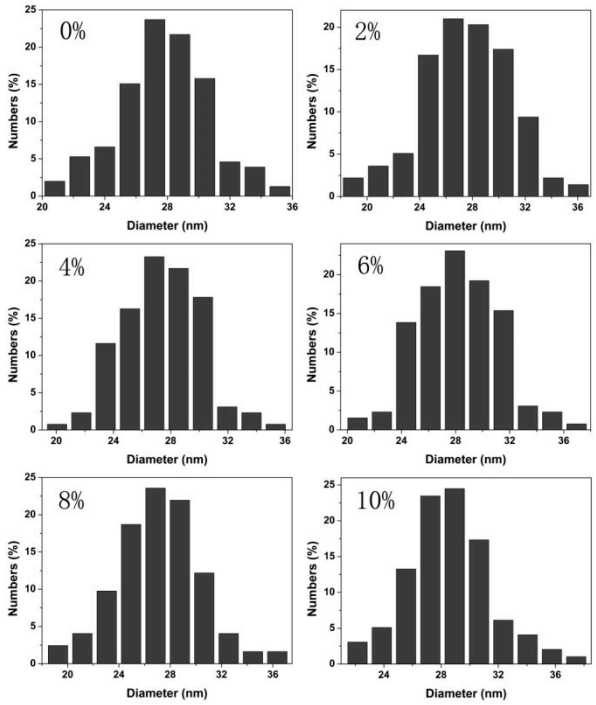

Figure 3. The TEM photo and the size distribution histogram of YF_3:Eu^{3+} nanocrystals.

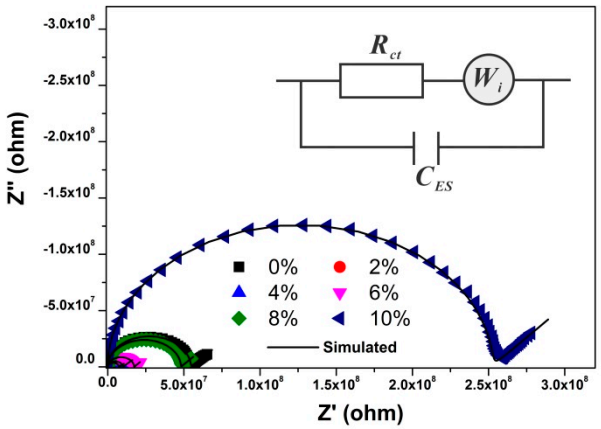

Figure 4. The impedance plots of YF_3:Eu^{3+} nanocrystals. The DC polarization voltage for the impedance plots (V_{DC}) is 0 V. The insert is the equivalent circuits, R_{ct} is the ion transfer resistance, W_i is Warburg element, C_{ES} is the capacitance between the sample and electrode.

Table 1. The fitting parameters of the equivalent circuit for the impedance plots.

Eu Concentration	R_{ct} (Ω)	C_{ES} (F)	W_i-R (Ω)	W_i-P	W_i-T (S)
0%	5.44×10^7	7.55×10^{-12}	8	0.260	7.50×10^{-12}
2%	9.90×10^6	6.55×10^{-12}	7	0.246	6.50×10^{-12}
4%	7.32×10^6	5.55×10^{-12}	6	0.235	5.55×10^{-12}
6%	1.73×10^7	7.95×10^{-12}	2	0.265	9.95×10^{-12}
8%	4.89×10^7	5.05×10^{-12}	3	0.265	5.50×10^{-12}
10%	2.52×10^8	5.05×10^{-12}	10	0.270	5.05×10^{-12}

To the Warburg diffusion process, the real impedance part ($Z^{'}$) in the low frequency region can be expressed as [29–31]:

$$Z' = Z_0' + \sigma\omega^{-1/2} \quad (1)$$

where σ is Warburg coefficient, Z_0' is constant and ω is frequency. By linear fitting the plots of Z'~$\omega^{-1/2}$ [as shown in Figure 5], the Warburg coefficient σ was obtained.

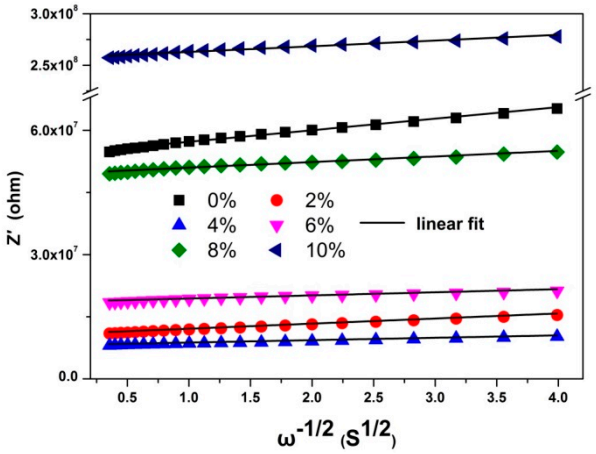

Figure 5. The Z'~$\omega^{-1/2}$ plots of YF_3:Eu^{3+} nanocrystals at low frequencies.

The diffusion coefficient of F^- ion can be gained by the following equation,

$$D_i = 0.5\left(\frac{RT}{AF^2\sigma C}\right)^2 \quad (2)$$

where R is the ideal gas constant, T is temperature, F is the Faraday constant, C is the molar concentration of ions. Let D_0 be the F^- ion diffusion coefficient of un-doped YF_3, then the D_i/D_0 of different Eu-doping concentration can be gained and was shown in Figure 6a.

By simulating the spectra with the equivalent circuit, the ion transfer resistances (R_{ct}) of YF_3 with different Eu-doping concentrations are obtained. The ionic conductivity σ_i can be gained by the following formula:

$$\sigma_i = \frac{d}{R_{ct}A} \quad (3)$$

where d is the sample thickness, and A is the electrode area. The Eu-doping concentration dependence of the ionic conductivity was shown in Figure 6b.

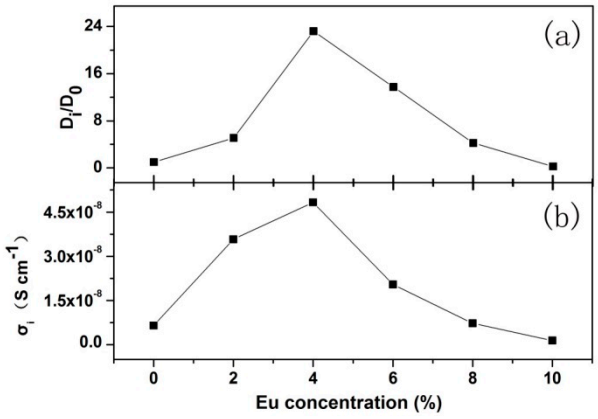

Figure 6. The variation of the ionic diffusion coefficient (**a**) and conductivity (**b**) with the Eu-doping concentration.

It can be seen that the ion diffusion coefficient and conductivity increase with the doping concentration until they reach 4% and then decrease. The changing mechanism of the two parameters can be interpreted as the following: the Eu^{3+} ionic radius is larger than that of Y^{3+}; while the size

mismatch will lead to the structural disorder and lattice strain [1], which finally deduces the increase of the ion diffusion coefficient and conductivity. When the doping concentration is larger than 4%, the interaction of the neighboring doping ions emerges due to the decrease of distance between them [32], which results in the difficulty of ion migration and finally causes the decreases of the ion diffusion coefficient and conductivity.

To further explore the carrier transport mechanism of YF_3:Eu^{3+}, its dielectric properties were investigated. The frequency dependence of the permittivity real part (ε'), imaginary part (ε'') and the dielectric loss tangent (tanδ) with different Eu^{3+} doping concentration were shown in Figure 7.

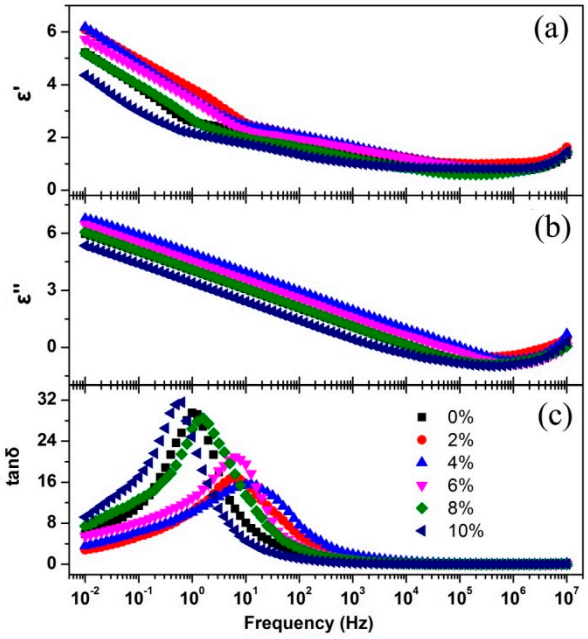

Figure 7. The frequency dependence of ε' (**a**), ε'' (**b**) and tanδ (**c**) with different Eu^{3+} doping concentration.

It can be seen that with frequency increasing ε' decreases sharply, then decreases slowly, and finally increases. ε'' decreases almost linearly with frequency increasing and then increases. The strong dispersion of the permittivity in the low frequency region indicates the charge carrier transport mechanism is the ion hopping in the system [33]. Ionic hopping behavior occurs as follows: under the action of electric field, one F^- ion moves to a more advantageous site (vacancy or interstitial position), then a vacancy is formed at this position and becomes an advantageous site to its surrounding atoms and so on. From Figure 7c, it can be seen that all the dielectric loss tangent plots show well-defined peaks in the frequency region of 0.1–100 HZ, which indicates the existence of the interfacial polarization between the grain boundaries in all of the samples. This loss peak distribution is in agreement with the Maxwell-Wagner relaxation model [34]. It can be deduced that the hopping dispersion in this region is affected by this interfacial polarization, and this phenomenon is similar to the result obtained from AC conduction investigation on YF_3 thin film conducted by Sathyamoorthy et al. [22]. From Figure 7, it can be concluded that with the increasing of ionic conductivity, the ε' and ε'' increase in the low frequency region and the loss peak of tanδ plot shifts to higher frequency. Before 4% Eu^{3+} doping, the structural disorder and lattice strain increase with the doping concentration increasing, which are beneficial for the ion migration, and finally result in the ion hopping becoming easier and the interfacial polarization relaxation frequency increasing. When the doping concentration is larger than 4%, the interaction of the neighboring doping ions is strengthened and its effect is dominated; the scattering to ions and dipoles enhances; which finally makes the ion hopping more difficult and makes the interfacial polarization relaxation frequency decrease.

4. Conclusions

The structure, component and morphology of YF_3:Eu^{3+} nanocrystals were measured by XRD, EDS and TEM. The ionic transportation and dielectric properties of YF_3:Eu^{3+} nanocrystals are investigated by AC impedance spectroscopy. The ion diffusion coefficient and conductivity increase with the doping concentration increasing and reach their highest values at 4% of Eu^{3+}. The difference of ionic radius between Eu^{3+} and Y^{3+} leads to the structural disorder and lattice strain, which deduces the increase of the ion diffusion coefficient and conductivity before 4% Eu^{3+} doping. Afterwards, the interaction of the neighboring doping ions is dominated, which results in the difficulty of ion migration and the decreases of the ion diffusion coefficient and conductivity. The strong dispersion of the permittivity in the low frequency region indicates that the charge carrier transport mechanism is the ion hopping in the system. The low-frequency hopping dispersion is affected by an interfacial polarization, which exhibits a Maxwell-Wagner relaxation process and its loss peak shifts to higher frequency with the ionic conductivity increasing. We have conducted a thorough study on the ionic transportation and dielectric properties of YF_3 nanocrystals with different Eu^{3+} doping concentration and it is hoped that the design of YF_3-based devices could benefit from this investigation.

Author Contributions: X.C. conceived and designed the experiments; J.W. and Y.C. fabricated and characterized the sample; X.Z. and J.Z. collaborated in XRD, TEM measurements; T.H., X.L., J.Y. and C.G. analyzed the data. All authors discussed the experiment results and contributed to writing the paper.

Funding: This research was funded by [the National Natural Science Foundation of China] grant numbers [11674404, 11704151, 21601062 and 11404137], [the Program for the development of Science and Technology of Jilin province] grant number [20180101206JC], [Thirteenth Five-Year Program for Science and Technology of Education Department of Jilin Province, China] grant numbers [JJKH20180772KJ and JJKH20180769KJ] and [Open Project of State Key Laboratory of Superhard Materials (Jilin University)] grant number [201710]

Conflicts of Interest: The authors declare no conflict of interest.

References

1. Breuer, S.; Lunghammer, S.; Kiesl, A.; Wilkening, M. F anion dynamics in cation-mixed nanocrystalline LaF_3:SrF_2. *J. Mater. Sci* **2018**, *53*, 13669–13681. [CrossRef]
2. Vetrone, F.; Capobianco, J.A. Lanthanide-doped fluoride nanoparticles: Luminescence, upconversion, and biological applications. *Int. J. Nanotechnol.* **2008**, *5*, 1306–1339. [CrossRef]
3. Chen, D.Q.; Yu, Y.L.; Wang, Y.S.; Huang, P.; Weng, F.Y. Cooperative Energy Transfer Up-Conversion and Quantum Cutting Down-Conversion in Yb^{3+}:TbF_3 Nanocrystals Embedded Glass Ceramics. *J. Phys. Chem. C* **2009**, *113*, 6406–6410. [CrossRef]
4. Zhang, M.F.; Fan, H.; Xi, B.J.; Wang, X.Y.; Dong, C.; Qian, Y.T. Synthesis, Characterization, and Luminescence Properties of Uniform Ln^{3+}-Doped YF_3 Nanospindles. *J. Phys. Chem. C* **2007**, *111*, 6652–6657. [CrossRef]
5. Lakshminarayana, G.; Yang, R.; Mao, M.; Qiu, J.; Kityk, I.V. Photoluminescence of Sm^{3+}, Dy^{3+}, and Tm^{3+}-doped transparent glass ceramics containing CaF_2 nanocrystals. *J. Non-Cryst. Solids* **2009**, *355*, 2668–2673. [CrossRef]
6. Yan, R.X.; Li, Y.D. Down/up conversion in Ln^{3+}-doped YF_3 nanocrystals. *Adv. Funct. Mater.* **2005**, *15*, 763–770. [CrossRef]
7. Sayed, F.N.; Grover, V.; Godbole, S.V.; Tyagi, A.K. Color tunable YF_3: Ce^{3+}/Ln($^{3+}$)(Ln($^{3+}$): Eu^{3+}, Tb^{3+}, Dy^{3+}, Sm^{3+}) luminescent system: Role of sensitizer and energy transfer study. *RSC Adv.* **2012**, *2*, 1161–1167. [CrossRef]
8. Tao, F.; Wang, Z.J.; Yao, L.Z.; Cai, W.L.; Li, X.G. Synthesis and Photoluminescence Properties of Truncated Octahedral Eu-Doped YF_3 Submicrocrystals or Nanocrystals. *J. Phys. Chem. C* **2007**, *111*, 3241–3245. [CrossRef]
9. Li, D.; Yu, W.S.; Dong, X.T.; Wang, J.X.; Liu, G.X. Synthesis and luminescence properties of YF_3:Eu^{3+} hollow nanofibers via the combination of electrospinning with fluorination technique. *J. Fluor. Chem.* **2013**, *145*, 70–76. [CrossRef]
10. Zhong, S.L.; Lu, Y.; Gao, M.R.; Liu, S.J.; Peng, J.; Zhang, L.C.; Yu, S.H. Monodisperse Mesocrystals of YF_3 and Ce^{3+}/Ln^{3+} (Ln = Tb, Eu) Co-Activated YF_3: Shape Control Synthesis, Luminescent Properties, and Biocompatibility. *Chem. Eur. J.* **2012**, *18*, 5222–5231. [CrossRef] [PubMed]
11. Peng, C.; Li, C.X.; Li, G.G.; Li, S.W.; Lin, J. YF_3:Ln^{3+} (Ln = Ce, Tb, Pr) submicrospindles: Hydrothermal synthesis and luminescence properties. *Dalton Trans.* **2012**, *41*, 8660–8668. [CrossRef] [PubMed]

12. Jia, G.; Huang, C.M.; Wang, C.Z.; Jiang, J.J.; Li, S.; Ding, S.W. Facile synthesis and luminescence properties of uniform and well-dispersed YF_3:Eu^{3+} architectures. *CrystEngComm* **2012**, *14*, 4425–4430. [CrossRef]
13. Réau, J.M.; Fedorov, P.P.; Rabardel, L.; Matar, S.F.; Hagenmuller, P. Phase equilibrium and ionic conductivity in the PbF_2-YF_3 system. *Mater. Res. Bull.* **1983**, *18*, 1235–1246. [CrossRef]
14. Patwe, S.J.; Balaya, P.; Goyal, P.S.; Tyagi, A.K. Ionic conductivity in solid solutions of PbF_2 and YF_3. *Mater. Res. Bull.* **2001**, *36*, 1743–1749. [CrossRef]
15. Adam, J.L. Lanthanides in Non-Oxide Glasses. *Chem. Rev.* **2002**, *102*, 2461–2476. [CrossRef] [PubMed]
16. Stouwdam, J.W.; Hebbink, G.A.; Huskens, J.; Van Veggel, F.C.J.M. Lanthanide-Doped Nanoparticles with Excellent Luminescent Properties in Organic Media. *Chem. Mater.* **2003**, *15*, 4604–4616. [CrossRef]
17. Lage, M.M.; Krambrock, K.; Moreira, R.L.; Gesland, J.Y. Infrared-spectroscopic study of orthorhombic YF_3 and LuF_3 single crystals. *Vib. Spectrosc.* **2005**, *39*, 244–248. [CrossRef]
18. Sarantopoulou, E.; Kollia, Z.; Cefalas, A.C. YF_3: Nd^{3+}, Pr^{3+}, Gd^{3+} wide band gap crystals as optical materials for 157-nm photolithography. *Opt. Mater.* **2001**, *18*, 23–26. [CrossRef]
19. Pankratov, V.; Kirm, M.; von Seggern, H. Intrinsic luminescence in yttrium trifluoride. *J. Lumin.* **2005**, *113*, 143–150. [CrossRef]
20. Gong, C.; Li, Q.J.; Liu, R.; Hou, Y.; Wang, J.X.; Dong, X.T.; Liu, B.; Yang, X.; Yao, Z.; Tan, X.; et al. Structural phase transition and photoluminescence properties of YF_3 and YF_3:Eu^{3+} under high pressure. *Phys. Chem. Chem. Phys.* **2013**, *15*, 19925–19931. [CrossRef] [PubMed]
21. Gong, C.; Li, Q.J.; Liu, R.; Hou, Y.; Wang, J.X.; Dong, X.T.; Liu, B.; Tan, X.; Liu, J.; Yang, K.; et al. Structural phase transition and photoluminescence properties of YF_3:Eu^{3+} nanocrystals under high pressure. *J. Phys. Chem. C* **2014**, *118*, 22739–22745. [CrossRef]
22. Sathyamoorthy, R.; Narayandass, S.K.; Balasubramanian, C.; Mangalaraj, D. Structure, Dielectric, and AC Conduction Studies on Yttrium Fluoride Thin Films. *Phys. Stat. Sol. A* **1990**, *117*, 495–500. [CrossRef]
23. Wang, J.; Yang, J.; Hu, T.; Chen, X.; Lang, J.; Wu, X.; Zhang, J.; Zhao, H.; Yang, J.; Cui, Q. Structural Phase Transition and Compressibility of CaF_2 Nanocrystals under High Pressure. *Crystals* **2018**, *8*, 199. [CrossRef]
24. Wang, J.S.; Cui, Q.L.; Hu, T.J.; Yang, J.H.; Li, X.Y.; Liu, Y.Q.; Liu, B.; Zhao, W.Q.; Zhu, H.Y.; Yang, L.L. Pressure-Induced Amorphization in BaF_2 Nanoparticles. *J. Phys. Chem. C.* **2016**, *120*, 12249. [CrossRef]
25. Wang, J.S.; Zhu, H.Y.; Ma, C.L.; Wu, X.X.; Zhang, J.; Li, D.M.; Cong, R.D.; Liu, J.; Cui, Q.L. High-Pressure Behaviors of SrF_2 Nanocrystals with Two Morphologies. *J. Phys. Chem. C.* **2013**, *117*, 615–619. [CrossRef]
26. Cui, X.Y.; Hu, T.J.; Wang, J.S.; Zhang, J.K.; Li, X.F.; Yang, J.H.; Gao, C.X. High pressure electrical transport behavior in SrF_2 nanoplates. *Chin. Phys. B* **2017**, *26*, 046401. [CrossRef]
27. Cui, X.Y.; Hu, T.J.; Wang, J.S.; Zhong, X.; Chen, Y.Z.; Zhang, J.K.; Li, X.F.; Yang, J.H.; Gao, C.X. Effect of Tb-doped Concentration Variation on the Electrical and Dielectric Properties of CaF_2 Nanoparticles. *Nanomaterials* **2018**, *8*, 532. [CrossRef] [PubMed]
28. Hu, T.J.; Cui, X.Y.; Wang, J.S.; Zhang, J.K.; Li, X.F.; Yang, J.H.; Gao, C.X. Transport properties of mixing conduction in CaF_2 nanocrystals under high pressure. *Chin. Phys. B* **2018**, *27*, 016401. [CrossRef]
29. Ho, C.; Raistrick, I.D.; Huggins, R.A. Application of A-C Techniques to the Study of Lithium Diffusion in Tungsten Trioxide Thin Films. *J. Electrochem. Soc.* **1980**, *127*, 343. [CrossRef]
30. Cui, X.Y.; Hu, T.J.; Wang, J.S.; Zhang, J.K.; Zhao, R.; Li, X.F.; Yang, J.H.; Gao, C.X. Mixed conduction in BaF_2 nanocrystals under high pressure. *RSC Adv.* **2017**, *7*, 12098–12102. [CrossRef]
31. Hu, T.; Cui, X.; Wang, J.; Zhong, X.; Chen, Y.; Zhang, J.; Li, X.; Yang, J.; Gao, C. The electrical properties of Tb-doped CaF_2 nanoparticles under high pressure. *Crystals* **2018**, *8*, 98. [CrossRef]
32. Li, D.; Dong, X.T.; Yu, W.S.; Wang, J.X.; Liu, G.X. Fabrication and luminescence of YF_3:Tb^{3+} hollow nanofibers. *J. Mater. Sci. Mater. Electron.* **2013**, *24*, 3041–3048. [CrossRef]
33. Peláiz Barranco, A.; Calderón Piñar, F.; Pérez Martínezy, O.; De Los Santos Guerra, J.; González Carmenate, I. AC behaviour and conductive mechanisms of 2.5 mol% La_2O_3 doped $PbZr_{0.53}Ti_{0.47}O_3$ ferroelectric ceramics. *J. Eur. Ceram. Soc.* **1999**, *19*, 2677–2683. [CrossRef]
34. Zhang, J.X.; Dai, J.Y.; Chan, H.L.W. Interfacial engineering and coupling of electric and magnetic properties in $Pb(Zr_{0.53}Ti_{0.47})O_3/CoFe_2O_4$ multiferroic epitaxial multilayers. *J. Appl. Phys.* **2010**, *107*, 104105. [CrossRef]